

Why grain in tree's trunks spirals: mechanical perspective

Seubpong Leelavanichkul and Andrej Cherkaev

Abstract The trunks of Ponderosa pine are curiously designed: Its grain spirals around the trunk. The natural question arises: Why does the evolution lead to such complication in the design? Here, we attempt to find the answer considering the morphology of a trunk as a result of the optimization of a mechanical construction. We model the trunk as an anisotropic cylinder with helicoidal symmetry, compute the stresses, and optimize the angle of the grain's inclination using a strength criterion. When the structure of the tree is optimized only for the strength, the objective remains practically neutral to the variation of the angle of spiraling if the angle does not exceed a limit, then the strength declines. The measured angle in the Ponderosa pine corresponds to this limit. Another biological factor must be considered: The transportation of the fluid from the roots to the branches. The spiraling is needed to achieve the uniform watering of the branches across the trunk even if the roots grow from one side only. The analysis of the stresses in the anisotropic cylinder with helicoidal symmetry under bending and compression loads is performed by introducing elastic potentials which generalize the potentials for cylindrical anisotropy.

Key words Spiral grain, Anisotropic elasticity, Wood failure, Biomimetics

1 Introduction

The paper concerns with morphology of tree's trunk from structural optimization viewpoint. Specifically, we investigate reasons behind spiral grows of Ponderosa Pine trunk in southern Utah. These trees develop helicoidal wood fibers that wiggle around the trunk as spirals. Spiral grain can be seen on many trees; they are visible when



Fig. 1 Ponderosa pine (photo by Cherkaev).

the bark is removed from the trunk; the angle is about $30^\circ - 50^\circ$. The question is why they twist. (Figure 1).

Many different reasons and hypotheses have been suggested to explain the spiraling, among them are such exotic factors as the earth rotation, the wind, and even the gravitational effect of the moon (Gedney (1986)). The theory worked out by Kubler Kubler (1991) provides a convincing qualitative reason for the spiraling. The tree's branches with straight grain are fed only by those roots directly below them. If the roots on either side of the tree are cut, then branches on that side will die when the grain is straight. In contrast, each root of a spiraling grain tree feeds nearly the whole tree. If all the roots on one side die, that side of the tree will still be healthy. This has been proven (Kubler (1991)) by injecting conifers with dye at the base. In addition to this consideration, trees become less stiff and bend more easily because of the spiraling grain. The bending allows trees to become more effective at discarding excessive snow from their branches and more resistant to breakage from heavy wind.

Received: date / Revised version: date

Seubpong Leelavanichkul and Andrej Cherkaev

Department of Mathematics, University of Utah, Salt Lake City, UT 84112 USA

This qualitative analysis, however, does not tell us how large the angle of the spiraling is. This paper performs stress analysis to estimate that angle. The structure of the paper is as follows. In the next section, we analyze the stresses in an anisotropic cylinder that models the tree's trunk. This stress analysis considers the structure under an axial loading and bending moment. The stresses are computed as a function of the grain angle. The objective is to determine the influence of the grain angle on the strength of the structure. To estimate the strength, the Tsai-Hill failure criterion is used.

The considered problem is an example of the inverse optimization problem (E. Cherkaev and A. Cherkaev (1999)) that arrives in evolution biology. Studying morphology like bones or trunks which are critical for the survival of a species, we may postulate that they are optimally adapted to the environment. Trees' trunks should stay unbroken and be able to sustain extreme wind loads applied from all directions. If a natural design becomes more complex, there must be a reason for this. We treat the evolutionary development of the species as the minimizing sequence of an optimization problem with unknown objective.

Notice that the optimization problems in engineering and in biology are mutually reciprocal. The biological structure is known, but it is not clear in what sense the structure is optimal. By contrast, the goal of the engineering is the minimization of a given functional that is not the subject of a search; the problem is to find an unknown optimal structure. This observation reflects the principal difference between biology that seeks an answer to the question: Why are the bio-materials and the biomimetics of living organisms the way they are and engineering that wants to know how to make an optimal structure.

2 Analysis

Before solving for the stress fields of this structure, we give a brief overview of equations required for the computation. Consider an infinite cylinder of the radius R , fulfilled by an orthotropic linear elastic material with the compliance \mathbf{S} , and loaded by bending moment M and the axial load P . We want to compute the stresses and further the strength of the cylinder and trace their dependence on the angle of twist of the anisotropic fulfillment. Assume that stresses inside the cylinder satisfy equations of linear elasticity:

$$\begin{aligned} 0 &= \nabla \cdot \boldsymbol{\sigma} \\ \boldsymbol{\sigma} &= \boldsymbol{\sigma}^T \\ \boldsymbol{\varepsilon} &= \mathbf{S} \cdot \boldsymbol{\sigma} \\ \boldsymbol{\varepsilon} &= \frac{1}{2} [\nabla \mathbf{u} + (\nabla \mathbf{u})^T] \end{aligned}$$

Consider differential element of the structure, the compliance of an orthotropic material can be expressed in

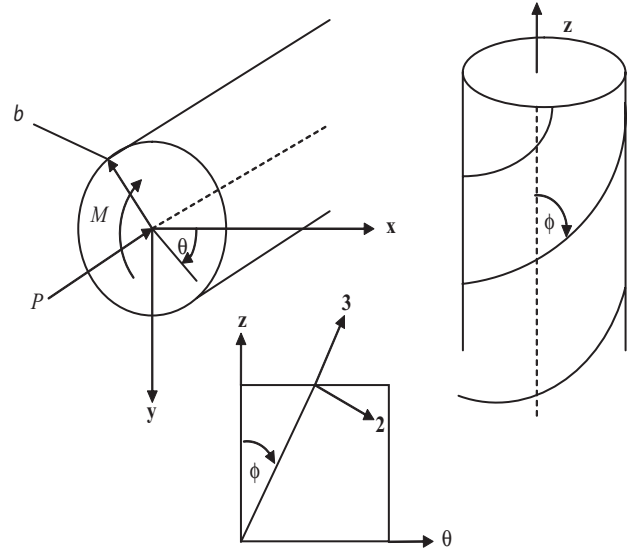


Fig. 2 Schematics of the tree trunk.

terms of the engineering elastic parameters. In the coordinates that coincide with principle axes of anisotropy tensor (direction of the grain), the Hooke's law takes the form:

$$\varepsilon_{ij}^* = S_{ijkl}^* \sigma_{ij}^*$$

where: ε_{ij}^* are strain components, including both normal and shear, σ_{ij}^* are stress components, including both normal and shear, and S_{ijkl}^* is the compliance matrix, or in the matrix form:

$$\begin{pmatrix} \varepsilon_{11}^* \\ \varepsilon_{22}^* \\ \varepsilon_{33}^* \\ \varepsilon_{23}^* \\ \varepsilon_{13}^* \\ \varepsilon_{12}^* \end{pmatrix} = \begin{bmatrix} \frac{1}{E_{11}} & -\frac{\nu_{21}}{E_{22}} & -\frac{\nu_{31}}{E_{33}} & 0 & 0 & 0 \\ -\frac{\nu_{21}}{E_{11}} & \frac{1}{E_{22}} & \frac{\nu_{32}}{E_{33}} & 0 & 0 & 0 \\ -\frac{\nu_{31}}{E_{11}} & \frac{\nu_{32}}{E_{22}} & \frac{1}{E_{33}} & 0 & 0 & 0 \\ 0 & 0 & 0 & \frac{1}{G_{23}} & 0 & 0 \\ 0 & 0 & 0 & 0 & \frac{1}{G_{13}} & 0 \\ 0 & 0 & 0 & 0 & 0 & \frac{1}{G_{12}} \end{bmatrix} \begin{pmatrix} \sigma_{11}^* \\ \sigma_{22}^* \\ \sigma_{33}^* \\ \sigma_{23}^* \\ \sigma_{13}^* \\ \sigma_{12}^* \end{pmatrix} \quad (1)$$

The subscript 1 represents the radial direction. Directions perpendicular and parallel to the grain are denoted by subscripts 2 and 3, respectively (see Figure 2).

2.1 Transformation of \mathbf{S}^*

The structure possesses cylindrical anisotropy. Hence, the analysis is conducted in cylindrical coordinates. It is needed to compute the components of (1) in the cylindrical system. The main coordinate axes of the compliance \mathbf{S}^* are directed as follows:

$$\begin{aligned} \mathbf{e}_r &= \mathbf{e}_1 \\ \mathbf{e}_\theta &= \cos \phi \mathbf{e}_2 + \sin \phi \mathbf{e}_3 \\ \mathbf{e}_z &= -\sin \phi \mathbf{e}_2 + \cos \phi \mathbf{e}_3 \end{aligned}$$

The new matrix can be written as:

$$\mathbf{S} = (\mathbf{K}^{-1})^T \mathbf{S}^* \mathbf{K}^{-1}$$

where \mathbf{S} is compliance matrix in cylindrical coordinates and \mathbf{K} is a rotation matrix. It has a block form (Ting (1996)):

$$\mathbf{K} = \begin{bmatrix} \mathbf{K}_1 & 2\mathbf{K}_2 \\ \mathbf{K}_3 & \mathbf{K}_4 \end{bmatrix} \quad (2)$$

where

$$\mathbf{K}_1 = \begin{bmatrix} \Omega_{11}^2 & \Omega_{12}^2 & \Omega_{13}^2 \\ \Omega_{21}^2 & \Omega_{22}^2 & \Omega_{23}^2 \\ \Omega_{31}^2 & \Omega_{32}^2 & \Omega_{33}^2 \end{bmatrix}$$

$$\mathbf{K}_2 = \begin{bmatrix} \Omega_{12}\Omega_{13} & \Omega_{13}\Omega_{11} & \Omega_{11}\Omega_{12} \\ \Omega_{22}\Omega_{23} & \Omega_{23}\Omega_{21} & \Omega_{21}\Omega_{22} \\ \Omega_{32}\Omega_{33} & \Omega_{33}\Omega_{31} & \Omega_{31}\Omega_{32} \end{bmatrix}$$

$$\mathbf{K}_3 = \begin{bmatrix} \Omega_{21}\Omega_{31} & \Omega_{22}\Omega_{32} & \Omega_{23}\Omega_{33} \\ \Omega_{31}\Omega_{11} & \Omega_{32}\Omega_{12} & \Omega_{33}\Omega_{13} \\ \Omega_{11}\Omega_{21} & \Omega_{12}\Omega_{22} & \Omega_{13}\Omega_{23} \end{bmatrix}$$

$$\mathbf{K}_4 = \begin{bmatrix} L_1 & L_2 & L_3 \\ L_4 & L_5 & L_6 \\ L_7 & L_8 & L_9 \end{bmatrix}$$

and

$$L_1 = \Omega_{22}\Omega_{33} + \Omega_{23}\Omega_{32}$$

$$L_2 = \Omega_{23}\Omega_{31} + \Omega_{21}\Omega_{33}$$

$$L_3 = \Omega_{21}\Omega_{32} + \Omega_{22}\Omega_{31}$$

$$L_4 = \Omega_{32}\Omega_{13} + \Omega_{33}\Omega_{12}$$

$$L_5 = \Omega_{33}\Omega_{11} + \Omega_{31}\Omega_{13}$$

$$L_6 = \Omega_{31}\Omega_{12} + \Omega_{32}\Omega_{11}$$

$$L_7 = \Omega_{12}\Omega_{23} + \Omega_{13}\Omega_{22}$$

$$L_8 = \Omega_{13}\Omega_{21} + \Omega_{11}\Omega_{23}$$

$$L_9 = \Omega_{11}\Omega_{22} + \Omega_{12}\Omega_{21}$$

Here Ω_{ij} are the elements of the matrix:

$$\mathbf{\Omega} = \begin{bmatrix} 1 & 0 & 0 \\ 0 & \cos \phi & \sin \phi \\ 0 & -\sin \phi & \cos \phi \end{bmatrix} \quad (3)$$

After the transformation, the matrix \mathbf{S} takes the following form:

$$\mathbf{S} = \begin{bmatrix} a_{11} & a_{12} & a_{13} & a_{14} & 0 & 0 \\ a_{21} & a_{22} & a_{23} & a_{24} & 0 & 0 \\ a_{31} & a_{32} & a_{33} & a_{34} & 0 & 0 \\ a_{41} & a_{42} & a_{43} & a_{44} & 0 & 0 \\ 0 & 0 & 0 & 0 & a_{55} & a_{56} \\ 0 & 0 & 0 & 0 & a_{65} & a_{66} \end{bmatrix}$$

where a_{ij} are the non-zero rotated elements that are determined from (2) and (3). Stresses and strains are transformed as following:

$$\boldsymbol{\sigma} = \mathbf{K}\boldsymbol{\sigma}^* \text{ and } \boldsymbol{\varepsilon} = (\mathbf{K}^{-1})^T \boldsymbol{\varepsilon}^*$$

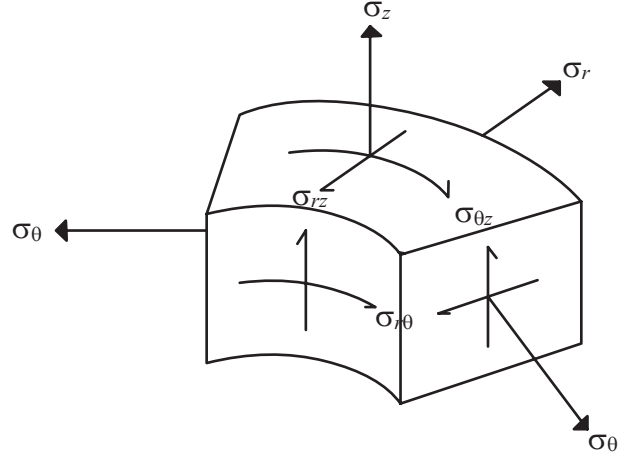


Fig. 3 Stress components in cylindrical coordinate

where: $\boldsymbol{\sigma}$ and $\boldsymbol{\varepsilon}$ are the stress and strain in the cylindrical coordinates.

Below, stresses are analyzed for two loading cases: axial loading and bending. Due to linearity of the model, the stresses are the sum of the results from these two loadings.

2.2

Stress functions

In this analysis, the body force is neglected; the cylinder is loaded from its ends. The cylindrical coordinate system as shown previously in Figure 2 is used. It is independent of z , Thus, the equilibrium equations in cylindrical coordinates become:

$$\frac{\partial \sigma_r}{\partial r} + \frac{1}{r} \frac{\partial \tau_{r\theta}}{\partial \theta} + \frac{\sigma_r - \sigma_\theta}{r} = 0$$

$$\frac{\partial \tau_{r\theta}}{\partial r} + \frac{1}{r} \frac{\partial \sigma_\theta}{\partial \theta} + \frac{2\tau_{r\theta}}{r} = 0$$

$$\frac{\partial \tau_{rz}}{\partial r} + \frac{1}{r} \frac{\partial \tau_{\theta z}}{\partial \theta} + \frac{\tau_{rz}}{r} = 0$$

and

$$\sigma_z = \frac{1}{a_{33}} (D - a_{13}\sigma_r - a_{23}\sigma_\theta - a_{34}\tau_{\theta z} - a_{35}\tau_{rz} - a_{36}\tau_{r\theta}) \quad (4)$$

where (see Lekhnitskii (1981)) $D = Br \sin \theta + C$. These four equations are bound together six components of the stress tensor $\sigma_r, \sigma_\theta, \sigma_z, \tau_{\theta z}, \tau_{rz}$, and $\tau_{r\theta}$ (see Figure 3). The other coefficients, B and C are the constants that are formed from the boundary conditions. To solve for the stress fields satisfying the equilibrium equations, two stress functions $\Phi(r, \theta)$ and $\Psi(r, \theta)$ are introduced as it is common in the theory of elasticity, (see for example Lekhnitskii (1981)). The stress components are expressed

through Φ and Ψ as:

$$\begin{aligned}\sigma_r &= \frac{1}{r} \frac{\partial \Phi}{\partial r} + \frac{1}{r^2} \frac{\partial^2 \Phi}{\partial \theta^2} \\ \tau_{r\theta} &= -\frac{\partial^2}{\partial r \partial \theta} \left(\frac{\Phi}{r} \right) & \sigma_\theta &= \frac{\partial^2 \Phi}{\partial r^2} \\ \tau_{\theta z} &= -\frac{\partial \Psi}{\partial r} & \tau_{rz} &= \frac{1}{r} \frac{\partial \Psi}{\partial \theta}\end{aligned}\quad (5)$$

Notice that σ_z is expressed through the other components by (4). According to Lekhnitskii (1981), the stress functions must satisfy the following equations:

$$\begin{aligned}L'_4 \Phi + L'_3 \Psi &= \frac{2}{a_{33}} (a_{13} - a_{33}) \frac{B \sin \theta}{r} \\ L''_3 \Phi + L'_2 \Psi &= \frac{2a_{34} B \sin \theta}{a_{33}} + \frac{a_{34} C}{r} - 2\xi\end{aligned}\quad (6)$$

where L'_4, L'_3, L''_3 , and L'_2 are differential operators of the fourth, third, and second orders, respectively:

$$\begin{aligned}L'_4 &= \beta_{22} \frac{\partial^4}{\partial r^4} + (2\beta_{12} + \beta_{66}) \frac{1}{r^2} \frac{\partial^4}{\partial r^2 \partial \theta^2} + \beta_{11} \frac{1}{r^4} \frac{\partial^4}{\partial \theta^4} \\ &\quad + 2\beta_{22} \frac{1}{r} \frac{\partial^3}{\partial r^3} - (2\beta_{12} + \beta_{66}) \frac{1}{r^3} \frac{\partial^3}{\partial r \partial \theta^2} - \beta_{11} \frac{1}{r^2} \frac{\partial^2}{\partial r^2} \\ &\quad + (2\beta_{11} + 2\beta_{12} + \beta_{66}) \frac{1}{r^4} \frac{\partial^2}{\partial \theta^2} + \beta_{11} \frac{1}{r^3} \frac{\partial}{\partial r} \\ L'_3 &= -\beta_{24} \frac{\partial^3}{\partial r^3} - (\beta_{14} + \beta_{56}) \frac{1}{r^2} \frac{\partial^3}{\partial r \partial \theta^2} \\ &\quad + (\beta_{14} - 2\beta_{24}) \frac{1}{r} \frac{\partial^2}{\partial r^2} \\ L''_3 &= -\beta_{24} \frac{1}{r} \frac{\partial^3}{\partial r^3} - (\beta_{14} + \beta_{56}) \frac{1}{r^2} \frac{\partial^3}{\partial r \partial \theta^2} \\ &\quad - (\beta_{14} + \beta_{24}) \frac{1}{r} \frac{\partial^2}{\partial r^2} + (\beta_{14} + \beta_{56}) \frac{1}{r^3} \frac{\partial^2}{\partial \theta^2} \\ L'_2 &= \beta_{44} \frac{\partial^2}{\partial r^2} + \beta_{55} \frac{1}{r^2} \frac{\partial^2}{\partial \theta^2} + \beta_{44} \frac{1}{r} \frac{\partial}{\partial r}\end{aligned}$$

and

$$\beta_{ij} = a_{ij} - \frac{a_{i3} a_{j3}}{a_{33}}$$

is the reducing strain coefficient. The derivations of these differential operators and their explicit forms are given in Lekhnitskii (1981).

2.3 Stresses due to axial loading

In the case of axial loading, the stress functions and the components of stress depend only on r . Thus, the solution to (6) and (7) are sought in the forms:

$$\Phi = f(r) \quad \Psi = g(r) \quad (8)$$

Therefore, parameter in the right-hand side of (6) and (7) is zero. Substituting (8) into (6) and (7), the following system of differential equations are obtained:

$$\begin{aligned}0 &= \beta_{22} f^{IV} + \frac{2\beta_{22}}{r} f''' \\ &\quad - \frac{\beta_{11}}{r^2} f'' + \frac{\beta_{11}}{r^3} f' - \beta_{24} g''' + \frac{(\beta_{14} - 2\beta_{24})}{r} g'' \\ \frac{a_{34} C}{r} - 2\xi &= \\ &\quad \beta_{24} f''' + \frac{(\beta_{14} + \beta_{56})}{r^2} f' + \beta_{44} g'' + \frac{\beta_{44}}{r^2} g'\end{aligned}\quad (9)$$

We look for the solutions to the homogeneous part of (9) and (10) in the forms:

$$f_h = F r^\alpha \quad g_h = G r^{\alpha-1} \quad (11)$$

The subscript h denotes a homogeneous solution. By substituting (11) into (9) and (10), r is eliminated, and we obtain a system:

$$\underbrace{\begin{bmatrix} H_1(\alpha) & H_2(\alpha) \\ H_3(\alpha) & H_4(\alpha) \end{bmatrix}}_{\mathbf{H}} \begin{bmatrix} F \\ G \end{bmatrix} = \begin{bmatrix} 0 \\ 0 \end{bmatrix} \quad (12)$$

The homogeneous system has nontrivial solution F and G only if $\det(\mathbf{H}) = 0$. Solving this relation, we obtain 6 parameters for $\alpha : 0, 0, 1, 2, \alpha_5$, and α_6 . The stress functions can now be expressed as:

$$\begin{aligned}\Phi &= (m_1 + m_2 \ln r + m_3 r + m_4 r^2 + m_5 r^{\alpha_5} + m_6 r^{\alpha_6}) \\ &\quad + \Phi_p\end{aligned}\quad (13)$$

$$\begin{aligned}\Psi &= (p_1 r^{-1} + p_2 r^{-1} \ln r + p_3 + p_4 r + p_5 r^{\alpha_5-1} + p_6 r^{\alpha_6-1}) \\ &\quad + \Psi_p\end{aligned}\quad (14)$$

where $m_1 \dots m_6, p_1 \dots p_6$ are the constants. Φ_p and Ψ_p are the particular solutions: $\Phi_p = a_1 r^3$ and $\Psi_p = b_1 r^2 + c_1 r$.

Consider the condition at point $r = 0$, one can see that $m_2 = m_3 = m_4 = p_1 = p_2 = p_4 = 0$ in order to avoid the singularity at this location. Moreover, any value of α_i that has a negative sign is discarded because stresses have to be finite. In this case, either α_5 or α_6 has a negative value. Let us assign these values to α_5 , so that $m_5 = p_5 = 0$. The stress functions now become:

$$\Phi = m_6 r^{\alpha_6} + \Phi_p \quad \Psi = p_6 r^{\alpha_6-1} + \Psi_p$$

The unknown constants are determined from the boundary conditions:

$$\sigma_r = \tau_{r\theta} = \tau_{\theta z} = \tau_{rz} = 0 \text{ at } r = b. \quad (15)$$

Utilizing (15), we have two equations with two unknowns. The constants in the particular solutions are determined from the end conditions:

$$\int_0^b \sigma_z r dr = \frac{P}{\pi b^2} \quad \int_0^b \tau_{\theta z} r^2 dr = 0$$

where P is the axial loading and b is the radius of the cylinder. Once all the constants are determined, stress components can then be evaluated according to (5). Because of the spiral anisotropy, the axial loading causes the cylinder to twist. The displacements are not computed in this analysis, since the main objective is to determine the stresses.

2.4 Stresses due to bending

Let us analyze the case where the structure is in pure bending. A bending moment M is applied at each end (Figure 2). The analysis still follows the same procedures as in axial loading case with the different stress functions:

$$\Phi = f(r) \sin \theta \quad \Psi = g(r) \sin \theta$$

In the pure bending case C and ξ in (6) and (7) are zero. Substituting the above stress functions into (6) and (7), the following systems of differential equations are obtained:

$$\begin{aligned} \frac{2(a_{13} - a_{33})B}{a_{33}r} = & \beta_{22}f^{IV} - \frac{(2\beta_{12} + \beta_{66})}{r^2}f'' + \frac{\beta_{11}}{r^4}f + \frac{2\beta_{22}}{r} \\ & + \frac{(2\beta_{12} + \beta_{66})}{r^3}f' - \frac{\beta_{11}}{r^2}f'' - \frac{(2\beta_{11} + 2\beta_{12} + \beta_{66})}{r^4}f \\ & + \frac{\beta_{11}}{r^3}f' - \beta_{24}g''' + \frac{(\beta_{14} + \beta_{56})}{r^2}g + \frac{(\beta_{14} - 2\beta_{24})}{r}g'' \\ \frac{2a_{34}B}{a_{33}} = & -\beta_{24}f''' + \frac{(\beta_{14} + \beta_{56})}{r^2}f' - \frac{(\beta_{14} + \beta_{24})}{r}f'' \\ & - \frac{(\beta_{14} + \beta_{56})}{r^3}f + \beta_{44}g'' + \frac{\beta_{55}}{r^2}g + \frac{\beta_{55}}{r^2}g' \end{aligned} \quad (16)$$

Similar to the axial loading case, the solutions to the homogeneous part of (16) and (17) assume the forms of (11), and α is solved as described in the axial loading case using (12). Solving (12) yields six values: 1, 1, α_3 , α_3 , α_4 , α_5 , and α_6 . The stress functions can now be expressed as:

$$\begin{aligned} \Phi = & (m_1r + m_2r \ln r + m_3r^{\alpha_3} + m_4r^{\alpha_4} + m_5r^{\alpha_5} + \\ & m_6r^{\alpha_6}) \sin \theta + \Phi_p \\ \Psi = & (p_1 + p_2 \ln r + p_3r^{\alpha_3-1} + p_4r^{\alpha_4-1} + p_5r^{\alpha_5-1} + \\ & p_6r^{\alpha_6-1}) \sin \theta + \Psi_p \end{aligned}$$

where $\Phi_p = a_1r^3 \sin \theta$ and $\Psi_p = b_1r^2 \sin \theta$. Once again, by setting the condition at $r = 0$, one can see that m_2 and p_2 are zero, and as in the axial loading case, any

value of α_i that has a negative sign is omitted. Now, the stress functions become:

$$\begin{aligned} \Phi &= (m_3r^{\alpha_3} + m_4r^{\alpha_4}) \sin \theta + \Phi_p \\ \Psi &= (p_3r^{\alpha_3-1} + p_4r^{\alpha_4-1}) \sin \theta + \Psi_p. \end{aligned}$$

The unknown constants m_3 , m_4 , p_3 , and p_4 are determined from the boundary conditions:

$$\sigma_r = \tau_{r\theta} = \tau_{\theta z} = \tau_{rz} = 0 \text{ at } r = b. \quad (18)$$

Utilizing (18), a system of four equations and four unknowns is obtained. The constants in the particular solutions are determined from the end conditions:

$$\begin{aligned} \int_0^{2\pi} \int_0^b \sigma_z r^2 \sin \theta dr d\theta &= M \\ \int_0^{2\pi} \int_0^b \sigma_z r^2 \cos \theta dr d\theta &= 0. \end{aligned}$$

Finally, stress components can then be evaluated according to (5). This computation was carried out using Maple V. This analysis enables us to compute stresses in an anisotropic elastic cylinder with rotated axes of anisotropy. Although the calculations are analytic, the resulting formulas (obtained by Maple V) are bulky and we do not display them here.

2.5 Failure criteria

Due to the nature of the anisotropy, the conventional maximum strength criterion for isotropic materials gives a poor prediction of failure (Swanson (1997)). For wood, we use Tsai-Hill failure criterion:

$$\left(\frac{\sigma_1}{\sigma_{1u}}\right)^2 + \left(\frac{\sigma_2}{\sigma_{2u}}\right)^2 - \frac{\sigma_1\sigma_2}{\sigma_{1u}^2} + \left(\frac{\tau_{12}}{\tau_{12u}}\right)^2 < 1 \quad (19)$$

When the left hand side of (19) is greater than or equal to 1, the failure is predicted. No distinction is made between compressive and tensile stresses.

Another criterion that is often used for wood structure is Hankinson's formula (Gedney (1986)):

$$\sigma_u = \frac{\sigma_{1u}\sigma_{2u}}{\sigma_{1u} \sin^2 \phi + \sigma_{2u} \cos^2 \phi}$$

Hankinson's formula approximates the ultimate axial strength as a function of the grain angle.

3 Analysis of Ponderosa pine

Based on the pure mechanical model presented in the previous section, the stresses were determined for Ponderosa pine. First, the stresses were computed for the

Table 1 Elastic moduli of Ponderosa pine with 12 % moisture content, 10^6 psi.

| E_1 | E_2 | E_3 | G_{12} | G_{13} | G_{23} |
|--------|--------|-------|----------|----------|----------|
| 0.1236 | 0.0743 | 1.423 | 0.00994 | 0.1035 | 0.0978 |

case of axial loading and then the case of a bending moment. The computation of stresses demonstrates whether spiraling is related to the elastic properties of the tree. If nature has already optimized the structure of living organisms, one expects the structure of the tree be optimized for the environment surrounding it. For instance, the structure of the tree should be in the configurations that maximize its strength to support the weight of branches, leaves, snow, and also resistance to the wind.

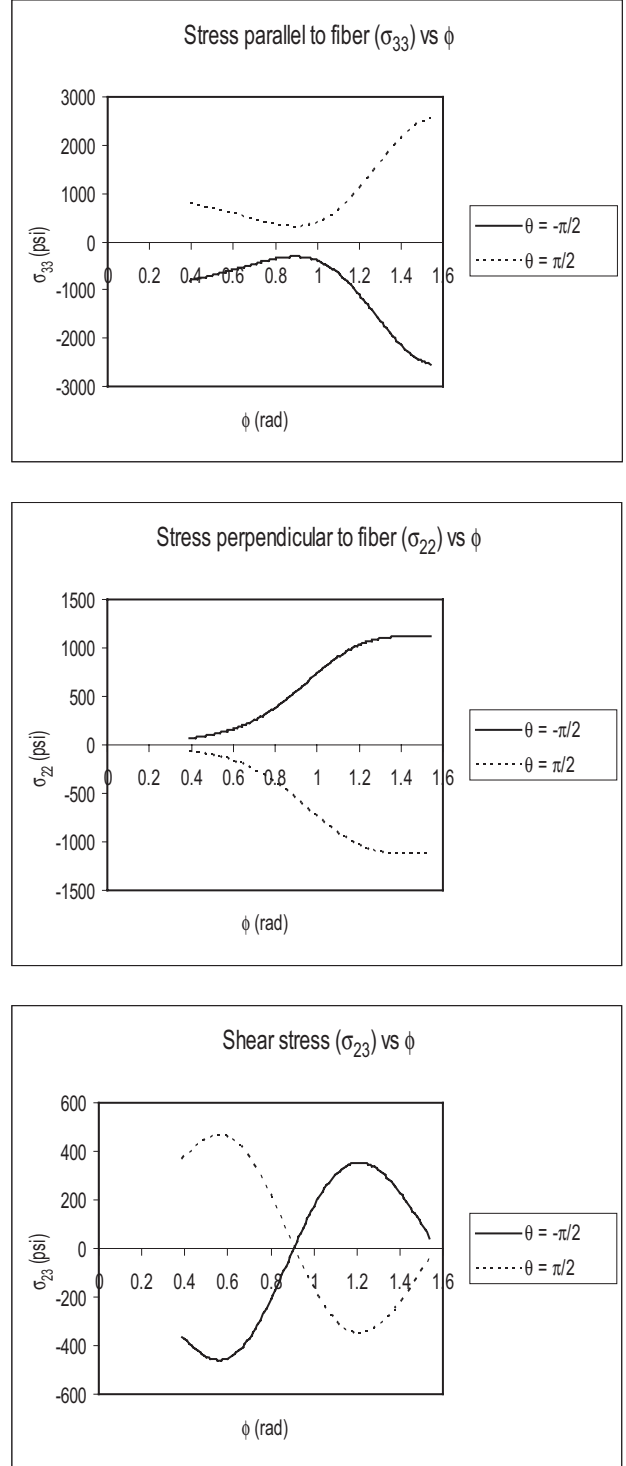
3.1 Setting of the parameters

We assumed that the trunk of the Ponderosa pine is cylindrical with radius $r = 10$ in. In addition, the axial loading is only a result of the weight and has the magnitude $P = 1500$ lb. The bending moment is approximated 10000 lb·in from the wind force. All the parameters are approximated in English unit in order to apply directly to the data that were obtained for Ponderosa pine. Table 1 shows the properties of the Ponderosa pine (Bodig and Jayne (1996)). Material strengths are (The Forest Products Laboratory (1955)): $\sigma_{33t} = 6300$ psi, $\sigma_{33c} = -5270$ psi, $\sigma_{22t} = 400$ psi, $\sigma_{22c} = -740$ psi, $\tau_{23ul} = 1160$ psi.

Utilizing this information, the calculation of stresses was performed. In this case, if the spiral angle is less than 21.2° , some α 's in (13) and (14) become negative. This leads to singularity at the center of the trunk at which $r = 0$. As a result, we only look at the grain angle ϕ that varies from 21.2° to 90° . Applying (19), we can predict when the structure fails.

3.2 Results

Figure 4 shows the total stresses resulting from bending and axial loading. Here, we look at the stresses and the maximal grain angle of Ponderosa pine using data and criteria given in Section 2.5 and Section 3.1. In addition, stresses are only investigated on the surface at $\theta = 90^\circ$ and $\theta = -90^\circ$ because maximum compressive and tensile stresses are expected at these locations. Only the plots of the stress fields are illustrated due to the size of the stress equations. Since P and M were arbitrary chosen, it is interesting to see how the failure prediction would vary if P or M changes. It is appropriate to vary M since the speed of the wind varies more than the weight on top of the tree. The grain angle and the Tsai-Hill minimum failure values are shown in Figure 5.

**Fig. 4** Total stresses on the surface of the tree.

As the magnitude of the bending moment increases, the maximal grain angle becomes smaller in order to reduce the bending stress. Maximal grain angle is approximately 37° (Figure 5). At this grain angle, the Ponderosa pine fails when the magnitude of the bending moment increases to 800 kip·in. Naturally, trees are uprooted when wind load is high. The stresses produced by the wind

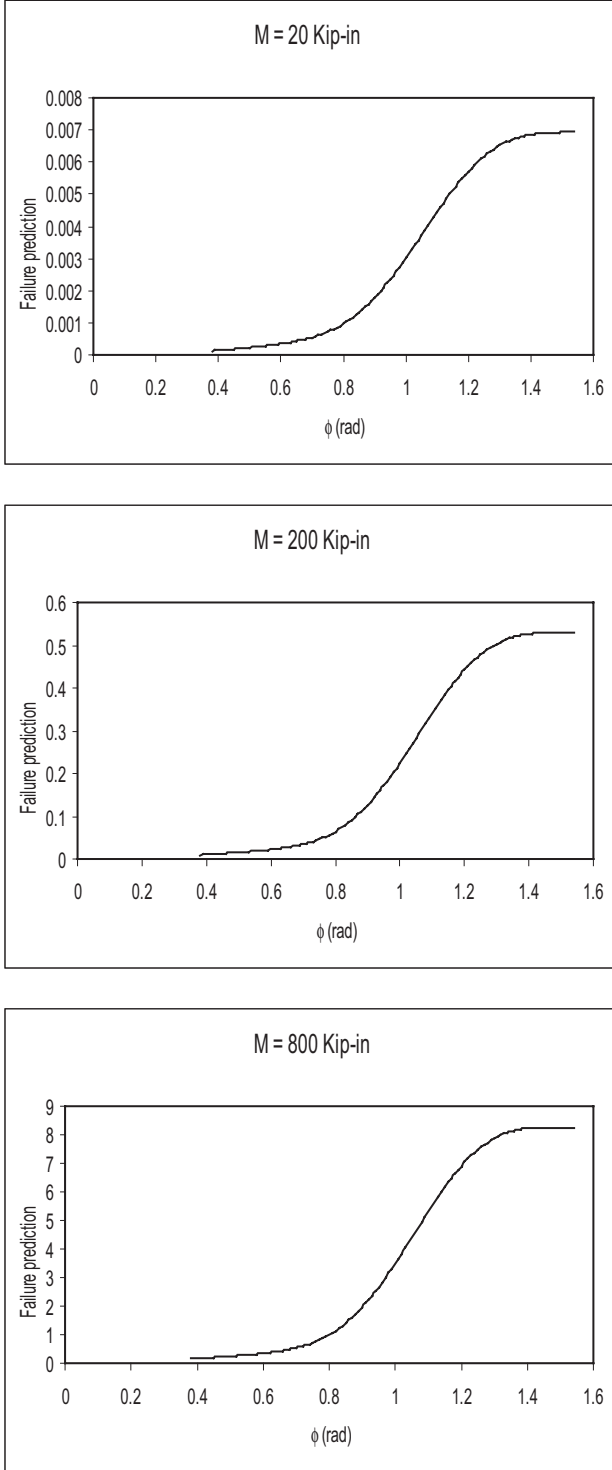


Fig. 5 Failure prediction using Tsai-Hill criterion at $\theta = \frac{\pi}{2}$.

load in nature are not typically high enough to exceed the strength of this tree. The ultimate strength of the Ponderosa pine is shown in Figure 6 using Hankinson's formula and Tsai-Hill failure criterion.

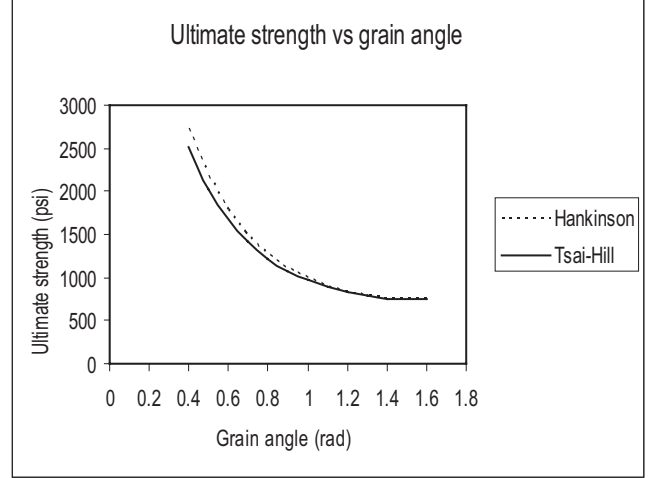


Fig. 6 Ultimate strength of Ponderosa pine at various spiral angles.

4 Structural optimization

In the beginning, we mentioned that the spiraling allows the fluid to be transferred throughout the whole tree even though the roots on one side has died. However, the presence of the spiraling also causes the tree to become less stiff. Hence, we need to determine the maximum grain angle that does not affect the strength of the tree significantly.

Having obtained the results of the failure predictions, one may use them to gain the benefits of the biomimetics of these trees. From Figure 5, we can see that the curves from these plots have the same shape but with the different in magnitudes. These curves show that there is a sharp increase in magnitude beyond 37° . From this observation, one could set up the problem of finding maximum angle as a problem of optimization with constraints as following:

Maximize the angle ϕ ($0 \leq \phi \leq \frac{\pi}{2}$) subject to the conditions

1. Failure criterion (19) is satisfied
2. Parameters of materials and loadings are as described in Section 3.1
3. The angle ϕ is within the range preceding the point where the sharp increase of the slope in Figure 5 takes place.

5 Discussion and conclusions

From this analysis, one cannot fully explain the relationship between the spiral twist and the mechanical properties of the tree; it is more reasonable to assume that the spiraling has to deal with fluid transportation. Instead,

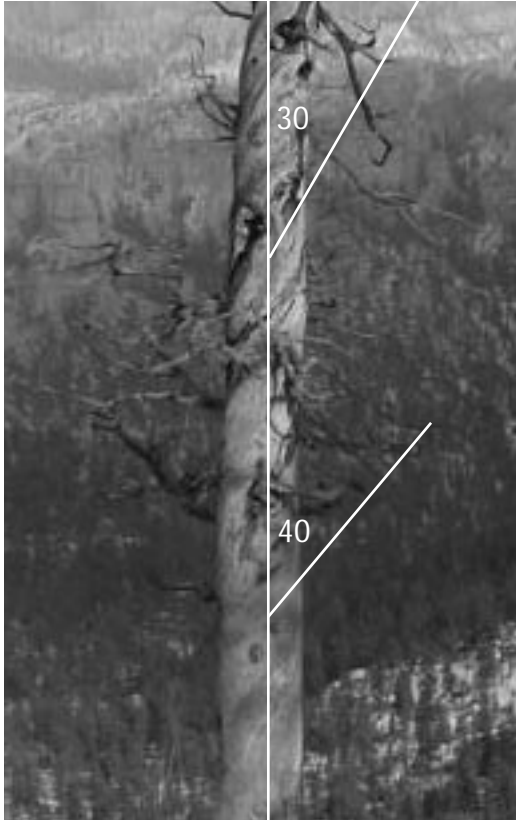


Fig. 7 Angle measurements at the lower and upper portion of the trunk.

it might be more appropriate to ask how big the angle could be in order for the tree to remain strong. Excessive spiraling not only reduces the stiffness of the tree but also weakens the strength of the tree. Hence, there ought to be a limiting point on how much the stiffness can be reduced in order for a tree to stand up straight. Its chance against breaking would increase if the tree does not bend enough.

The result from Figure 5 shows that the failure prediction value increases slowly to about 37° , and then the slope increases dramatically beyond this point. The tree strength is not sacrificed considerably, as long as the grain angle remains below 37° . The grain angle of the Ponderosa pine obtained using theory of anisotropic elasticity is slightly different from the angle measured in Figure 7. However, this was expected since many assumptions were made during the analysis. The permitted interval according to our analysis is between 21.2° and 37° .

Another observation made was the differences between the lower and the upper portion of the tree (Figure 7). The grain angle is bigger toward the bottom. When the tree is small, it requires more distribution of fluid to ensure proper growth. Having the fiber spiral at a bigger angle allows the tree to transport more fluid along its circumference. As the tree grows taller, the angle becomes smaller, which allows the fluid to be transported

to the higher portion faster by reducing the coverage area. This could be another reason why the grain angle varies this way. Details about the fluid transportation are not discussed here since it is beyond the scope of this analysis.

We did not consider the cracking of the trunk in our analysis which maybe an important factor. Looking at the elastic constants of Ponderosa pine, one finds that E_2 is approximately 5% of E_3 , which is almost as there is a crack. With this in mind, Leonid Slepyan (via private communication) has pointed out that, as the crack wiggles around the tree, it is less prone to fracture than when the crack is vertically straight.

Due to lack of information and actual data; for example, the average wind load and the load that can uproot the Ponderosa pine, it is not possible to give a solid conclusion regarding relationships between the magnitude of the twist and the elastic properties of trees. In addition, the results presented in this analysis only reflect the Ponderosa pine.

Our analysis shows that the question of the adaptation of a tree trunk can be viewed as a problem of constrained minimization. The spirals in the grain are developed for the non-mechanical reasons (e.g. transport of the water to branches) and the strength analysis provides a constraint that limits the angle of these spirals. In short, a structure can be more flexible by having the fibers spiral along its circumference. However, depending on the elastic properties of the material, the angle of the spiral can vary.

6

Acknowledgements

We are indebted to many people who encouraged us and advised us on different aspects of the modelling and analysis. Their general comments and suggestions were sound and worthwhile. Particularly, we mention the help from Tim Foliass, Stephen Swanson, Leonid Slepyan, Steve Cowin, Jack H.T. Chang, and Natalya Kizilova. One special thanks to Roderic Lakes, who offered numerous suggestions on the first draft. The problem was presented for discussion on our website <http://www.math.utah.edu/~cherk>, and we enjoyed numerous comments from colleagues, whom we are thankful. The work was sponsored by National Science Foundation (NSF Grant No: DMS- 0072717).

References

- Bodig, J. and Jayne, B. A.**, *Mechanics of Woods and Wood Composites* (Van Nostrand Reinhold, New York 1982)
- Cherkaev, E. and Cherkaev, A.**, Structural optimization and biological "designs". In: *Solid Mechanics and its Applications, v. 69: Synthesis in Bio Solid Mechanics*. M.Bendsoe and P.Pedersen eds. (Kluwer Academic Press, Dordrecht 1999) 247-264.

The Forest Products Laboratory, *Wood Handbook, No. 19* (U.S. Department of Agriculture, Washington, D.C.) 76

Gedney, L., Alaska Science Forum **Art 783**, (1986).

Kubler, H., *Trees* **5**, (1991) 125-135.

Lekhnitskii, S. G., *Theory of Elasticity of an Anisotropic Body* (MIR Publishers, Moscow 1981)

Swanson, S. R., *Introduction to Design and Analysis with Advanced Composite Materials* (Prentice-Hall, New Jersey 1997)

Ting, T. C. T., *Anisotropic Elasticity: Theory and Applications* (Oxford University Press, New York 1996)